AD-A114 603 AEROSPACE CORP EL SEGUNDO CA SPACE SCIENCES LAB F/G 14/2
A SATELLITE-BORNE LIMB SCANNING ULTRAVIOLET SPECTROMETER FOR TH--ETC(U)
APR 82 J B PRANKE, A B CHRISTENSEN, F A MORSE F04701-81-C-0082
UNCLASSIFIED TR-0082(2940-04)-2 SD-TR-82-30 NL

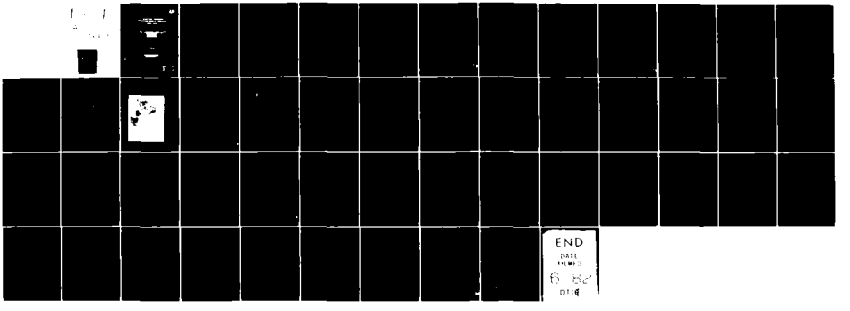

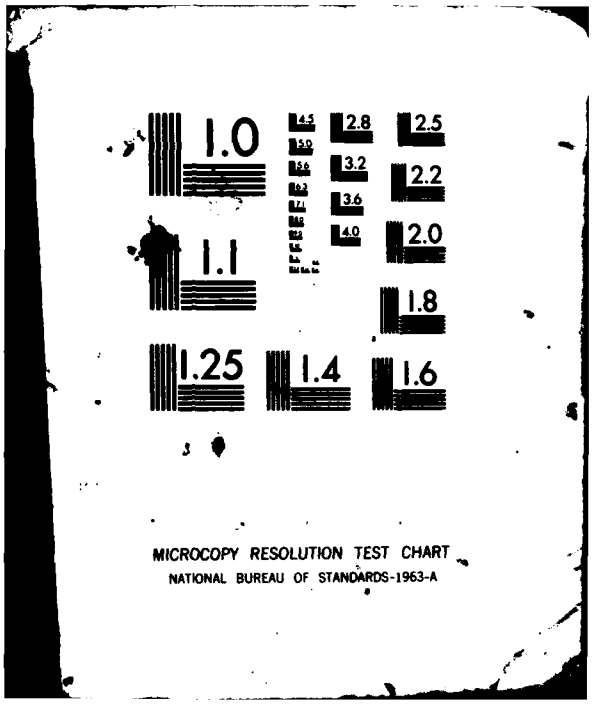
1.0
1.1
1.25
1.4
1.6
2.8
3.2
3.6
4.0
2.5
2.2
2.0
1.8
MICROCOPY RESOLUTION TEST CHART
NATIONAL BUREAU OF STANDARDS-1963-A

AD A114603

Prepared for
SPACE DIVISION
Air Force Systems Command
Los Angeles Air Force Station
P.O. Box 92960, Worldway Postal Center
Los Angeles, California 90009

DTIC
ELECTE
MAY 10 1982
S
D

82 05 10 044

This report was submitted by The Aerospace Corporation, El Segundo, CA 90245, under Contract No. F04701-81-C-0082 with the Space Division, Deputy for Technology, P.O. Box 92960, Worldway Postal Center, Los Angeles, CA 90009. It was reviewed and approved for The Aerospace Corporation by H. R. Rugge, Director, Space Sciences Laboratory.
was the project officer for the Mission-Oriented Investigation and Experimentation (MOIE) Program.

This report has been reviewed by the Public Affairs Office (PAS) and is releasable to the National Technical Information Service (NTIS). At NTIS, it will be available to the general public, including foreign nations.

This technical report has been reviewed and is approved for publication. Publication of this report does not constitute Air Force approval of the report's findings or conclusions. It is published only for the exchange and stimulation of ideas.

George A. Kuck, Major, USAF
Project Officer

Florian P. Mainhardt, Lt Col, USAF
Director, Advanced Space Development

FOR THE COMMANDER

Norman W. Lee, Jr., Col, USAF
Deputy for Technology

UNCLASSIFIED

SECURITY CLASSIFICATION OF THIS PAGE (When Data Entered)

REPORT DOCUMENTATION PAGE		READ INSTRUCTIONS BEFORE COMPLETING FORM
1. REPORT NUMBER SD-TR-82-30	2. GOVT ACCESSION NO. AD-A114	3. RECIPIENT'S CATALOG NUMBER 603
4. TITLE (and Subtitle) A SATELLITE-BORNE LIMB SCANNING ULTRAVIOLET SPECTROMETER FOR THERMOSPHERIC REMOTE SENSING		5. TYPE OF REPORT & PERIOD COVERED
		6. PERFORMING ORG. REPORT NUMBER TR-0082(2940-04)-2
7. AUTHOR(s) James B. Pranke, Andrew B. Christensen, F. A. Morse, David R. Hickman, William T. Chater, Charles K. Howey, and David A. Jones		8. CONTRACT OR GRANT NUMBER(s) F04701-81-C-0082
9. PERFORMING ORGANIZATION NAME AND ADDRESS The Aerospace Corporation El Segundo, Calif. 90245		10. PROGRAM ELEMENT, PROJECT, TASK AREA & WORK UNIT NUMBERS
11. CONTROLLING OFFICE NAME AND ADDRESS Space Division Air Force Systems Command Los Angeles, Calif. 90009		12. REPORT DATE 30 April 1982
		13. NUMBER OF PAGES 49
14. MONITORING AGENCY NAME & ADDRESS (if different from Controlling Office)		15. SECURITY CLASS. (of this report) Unclassified
		15a. DECLASSIFICATION/DOWNGRADING SCHEDULE

16. DISTRIBUTION STATEMENT (of this Report)

Approved for public release; distribution unlimited

17. DISTRIBUTION STATEMENT (of the abstract entered in Block 20, if different from Report)

18. SUPPLEMENTARY NOTES

19. KEY WORDS (Continue on reverse side if necessary and identify by block number)

EUV Spectrometer, Satellite, Remote Sensing, Airglow, Aurora

(DoD)

20. ABSTRACT (Continue on reverse side if necessary and identify by block number)

A concave grating Wadsworth spectrometer designed to scan the ultraviolet limb of the earth was flown on a ~~Defense Department meteorological~~ satellite to obtain measurements of atmospheric emissions in the wavelength range of 85 nm to 395 nm as a function of height above the solid earth.

The instrument field of view was 0.14 deg × 3.8 deg corresponding to 8 km in the vertical and 230 km in the horizontal at the limb. ~~The~~ scanning motion → prev)

DD FORM 1473 (FACSIMILE)

UNCLASSIFIED

SECURITY CLASSIFICATION OF THIS PAGE (When Data Entered)

19. KEY WORDS (Continued)

20. ABSTRACT (Continued)

was controlled by a momentum-compensated DC-torque motor mechanism that panned the line of sight across the limb corresponding to tangent altitudes of 80 km to 480 km. A set of three photon counting detectors, each viewing a separate exit slit, provided simultaneous coverage of the wavelength bands 85 to 120 nm (EUV), 110 to 163 nm (FUV) and 290 nm to 395 nm (UV), respectively. A separate photometric channel isolated the atmospheric sodium doublet at 589.0-589.6 nm.

The grating position and instrument view angle were controlled by digital circuitry operating on hardwired and uplinked command instructions. The operating modes included a variety of scanning and fixed wavelength and view angle operations.

A description of the instrument and several examples of the data are presented. These include the dayglow emissions from thermospheric oxygen and nitrogen that form the basis of a thermospheric density determination; auroral enhancements observed in these emissions and in hydrogen Ly α; and night-time sodium emissions.

Acknowledgments

The authors express their appreciation to Dr. George Paulikas and the management of the Space Sciences Laboratory for their support and encouragement in all phases of this project. We also wish to acknowledge the contribution of Dr. A. Prag to the experiment concept, Dr. E. Rogers and Mr. D. Vrabec to the optics design, and Mr. E. Erwin to the logic design. Our sincere appreciation is extended to Mr. B. Baldree and Mr. D. Watanabe for their technical efforts.

We thank Drs. C. Barth and K. Kelly at LASP for their generous assistance in the use of their calibration facilities.

This work was supported by the U. S. Air Force under Contract No. AF F07401-81-C-0082.

Accession For
NTIS GRA&I
DTIC TAB
Unannounced
Justification
By
Distribution/
Availability Codes
Dist | Avail and/or Special
A
COPY INSPECTED 2

CONTENTS

ACKNOWLEDGMENTS..... 1

I. INTRODUCTION..... 7

II. INSTRUMENT DESCRIPTION..... 11

III. OPTICAL DESIGN..... 15

IV. MECHANICAL DESIGN..... 23

V. ELECTRONIC DESIGN..... 25

VI. MODES OF OPERATION..... 31

VII. CALIBRATION..... 33

VIII. FLIGHT DATA..... 39

IX. CONCLUSIONS..... 47

REFERENCES..... 49

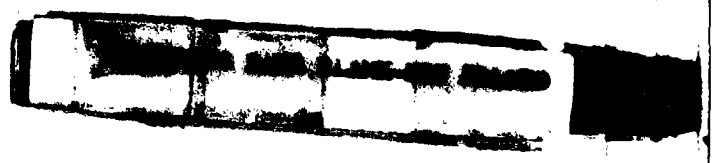

FIGURES

1.	Viewing Geometry for the SSD UV Limb Scanning Spectrometer.....	9
2.	Isometric Drawing Showing the Major SSD Systems.....	12
3.	Photograph of the SSD Instrument in the laboratory Test Fixture.....	13
4.	Diagram of the Modulation Collimator.....	16
5.	Block Diagram of the SSD Logic Circuits.....	26
6.	Interface Diagram Showing the Spacecraft and OLS (Operational Line Scan System) Interface Connections to the SSD Instrument.....	27
7.	Measured Blaze Efficienty of the SSD Flight Grating #233-4-2 Expressed as a Function of First-Order Wavelength.....	36
8.	Quantum Efficiencies for the Four Detector Channels.....	37
9.	Single Wavelength Scan of the Far Ultraviolet Dayglow (110-160 nm) for a Tangent Height of 210 km Obtained on Day 169 (18 June 1979).....	40
10.	An EUV Composite Spectrum of the Dayglow Obtained by Summing Spectra from Several Target Altitude and Satellite Locations.....	41
11.	Single α-Scan Mode 1 Data for the Atomic Oxygen Emissions OI(130.4 nm) and OI(135.6 nm) and the Molecular Nitrogen LBH(0,4) Emission at 132.5 nm.....	42
12.	Single α-Scan Data for Atomic Sodium (NaD) Doublet Emissions...	44
13.	Raw Count Rate Data from Day 253 (10 September 1979) with SSD Instrument in Mode 5, i.e., 4 Wavelength Positions at 4 Alpha Positions.....	45

TABLES

1. SSD Collimator Parameters..... 17

2. Detector Characteristics..... 20

3. Results for EUV Low Reflectance Surface Coatings..... 21

4. D-Sensor Modes of Operation..... 32

5. D-Sensor Responsivity at Selected Wavelengths..... 34

6. α-Scan Depression Angles in Degrees..... 38

I. INTRODUCTION

The primary objective of the limb scanning Wadsworth spectrometer, designated as SSD (Special Sensor D), flown on the DMSP-F4 (Defense Meteorological Satellite Program) satellite, was to evaluate a remote sensing technique for determining vertical profiles of thermospheric composition and density at altitudes important for drag predictions. These profiles were to be derived and supplied to the USAF Air Weather Service (AWA) in support of its user community.

The technique depends on the measurement of near and far ultraviolet radiations emitted by thermospheric molecular nitrogen and atomic oxygen. In the high altitude (> 100 km) sunlit atmosphere, the ionizing component of solar radiation produces photoelectrons with sufficient energy to excite the resonance lines of atomic oxygen and many band systems in N_2. The emitted photons propagate through the atmosphere, subject to absorption and scattering which alter their direction and in some cases their wavelength. These transport processes are particularly important for limb-viewing geometry because of the long, almost horizontal, viewing paths through the atmosphere (~ 3000 km). Since in each stage of the production and transport processes the neutral composition and distribution play an important role, measurements of the emission profile may be used to deduce the neutral composition using known excitation, absorption, and scattering cross sections and appropriate models.

The remote sensing concept that eventually led to the satellite experiment was developed by Prag (1971) well before the first spectral measurements of the earth's extreme ultraviolet emissions were made (Carruthers and Page, 1972; Christensen, 1976, and before some relevant cross-section measurements

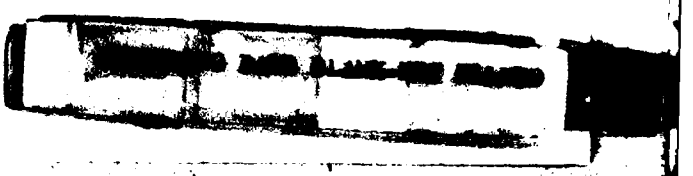

had been made. The final concept was based on measurements of the N_2 second positive (0,0) band emission at 337.1 nm. The band is populated primarily by photoelectron impact (Doering et al., 1970) with a threshold of approximately 11 eV, and the radiation is neither scattered nor absorbed in the thermosphere.

For determination of the oxygen density, emission at OI(135.6 nm) was selected. It is excited by photoelectron impact and absorbed in the Schumann-Runge continuum of O_2. Although it is not an electric dipole transition, there is sufficient resonance scattering of the radiation, especially below 200 km, to require multiple scattering effects be included in the analysis (Anderson et al., 1980).

The determination of the densities of N_2 and O was the major objective of the experiment but other processes of scientific and practical application were to be investigated. These secondary objectives included a description of the ultraviolet horizon in both the polar and equatorial regions at night and especially during times of enhanced emission from aurora.

The SSD instrument was launched on June 6, 1979, into a circular sun-synchronous orbit with a northbound equatorial crossing maintained at 2200 L.T. and an altitude of 830 km. The instrument was located on the underside of the satellite and viewed the earth's limb in the plane of the orbit and in the direction of satellite motion as shown in Figure 1. A narrow (0.14°) field of view in the vertical corresponds to an altitude spread of ~ 8 km at the tangent point, defined as the point of closest approach of the line of sight to the earth's surface. The instrument scanned the limb from approximately 80 km to 480 km corresponding to an angular rotation of the instrument of 8.5° on the 3-axis stabilized spacecraft. To keep the tangent point in

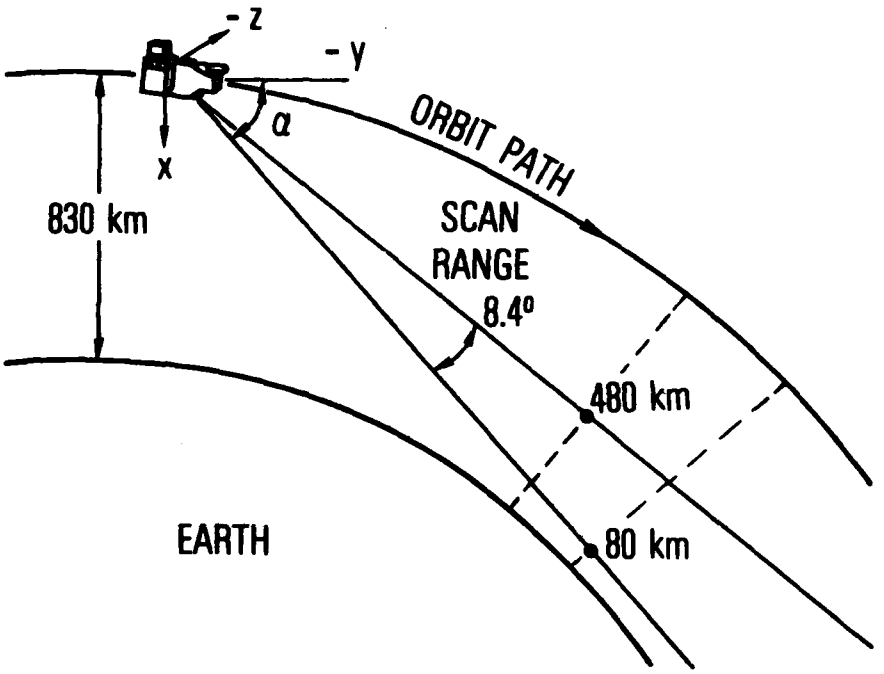

Fig. 1. Viewing Geometry for the SSD UV Limb Scanning Spectrometer. The satellite is in a circular, 830-km altitude, sun synchronous orbit with an inclination of 98.8°. It is 3-axis stabilized with the x-axis perpendicular to the local reference ellipsoid. The angle α scan nominally covers tangent heights from 80 km to 480 km.

roughly constant geographic position, the instrument was scanned from low to high altitude, thus compensating for satellite motion.

The design of the instrument was strongly influenced by a severe weight limitation resulting in a final instrument weight of 26.75 lbs. As a result, much difficulty was experienced with mechanical systems in qualification testing, and, despite design modifications to overcome the problems, there were some mechanical failures in flight that have reduced the quality and quantity of data for some emission features.

Section II gives an overall description of the instrument while sections III, IV and V cover the optical, mechanical and electrical aspects in more detail. The eight operating modes are described in detail in section VI. Calibration data for the optics, detectors and the altitude drive are provided in section VII and several examples of flight data are shown in section VIII.

II. INSTRUMENT DESCRIPTION

The instrument, illustrated in Figure 2, consists of a 0.5 m radius concave grating in a Wadsworth mount, a mechanical collimator to define the field of view, three fixed exit slits, and a set of photon counting detectors. There are three spectrometric channels: the far ultraviolet (FUV) from 110 nm to 163 nm in second order at 0.8 nm resolution, the extreme ultraviolet (EUV) from 85 nm to 120 nm in 3rd order at 0.4 nm resolution, and the near ultraviolet (UV) from 290 nm to 395 nm in first order at 1.2 nm resolution. The undiffracted central image is reflected by a dichroic mirror to a NaD detector.

The grating is rotated about an offset axis by a high-speed highly accurate mechanism (lambda drive servo) that provides for rapid motion and precise positioning of the grating. The system reproducibility is good to 0.02 degrees corresponding to less than 25% of a spectral resolution element.

The optics box, which includes the collimator, grating drive, detectors, etc., is connected via a shaft to the vertical limb scan (alpha scan) drive motor assembly as shown in the photograph (Figure 3). The alpha drive and the electronics box are rigidly attached to the spacecraft. Through both stored and telemetered commands, the alpha drive mechanism orients the instrument. Nominally line of sight tangent heights from 80 to 270 km are scanned in 6 km steps, while the range of tangent heights from 270 to 480 km is scanned in 25 km steps.

The operational control of the instrument is very flexible. Combinations of fixed and scanning modes of both the alpha and lambda drives are available. Counts are accumulated at each (α,λ) position for approximately one second.

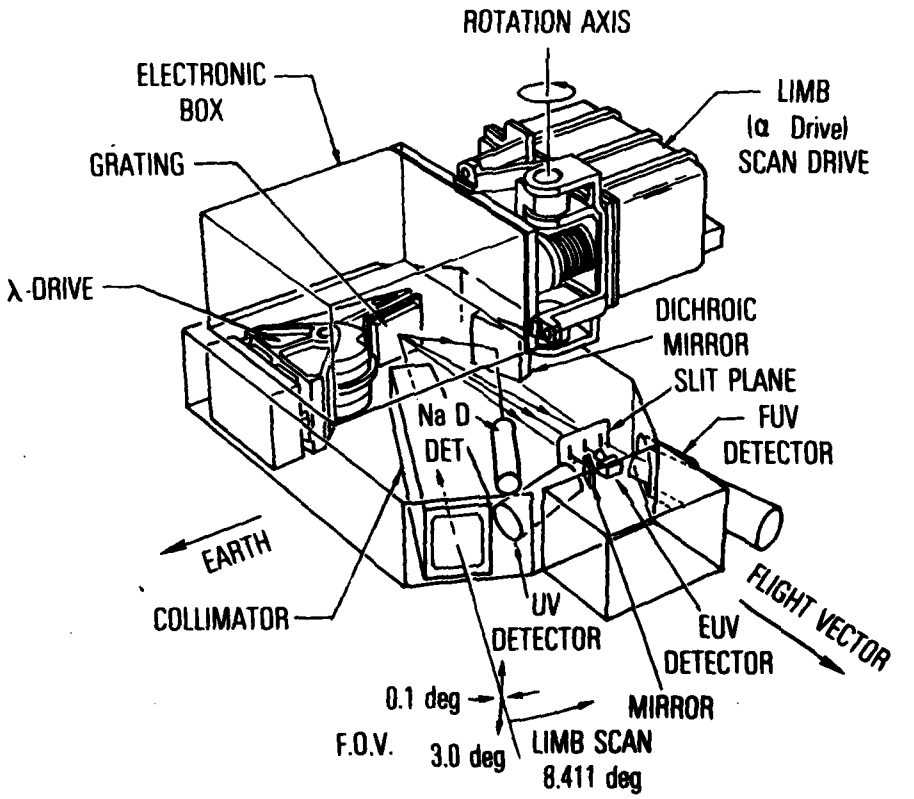

Fig. 2. Isometric Drawing Showing the Major SSD Systems. The limb scan drive and electronics box are mounted to the spacecraft. The optics box mounts to a shaft through the limb scan drive. The modulation collimator defines the field of view (0.14° × 3.5°). Light diffracted in the first order is focused on the near UV detector, second order on the FUV detector, and third order on the EUV detector. The undiffracted central image is directed to the dichroic mirror and onto the NaD detector.

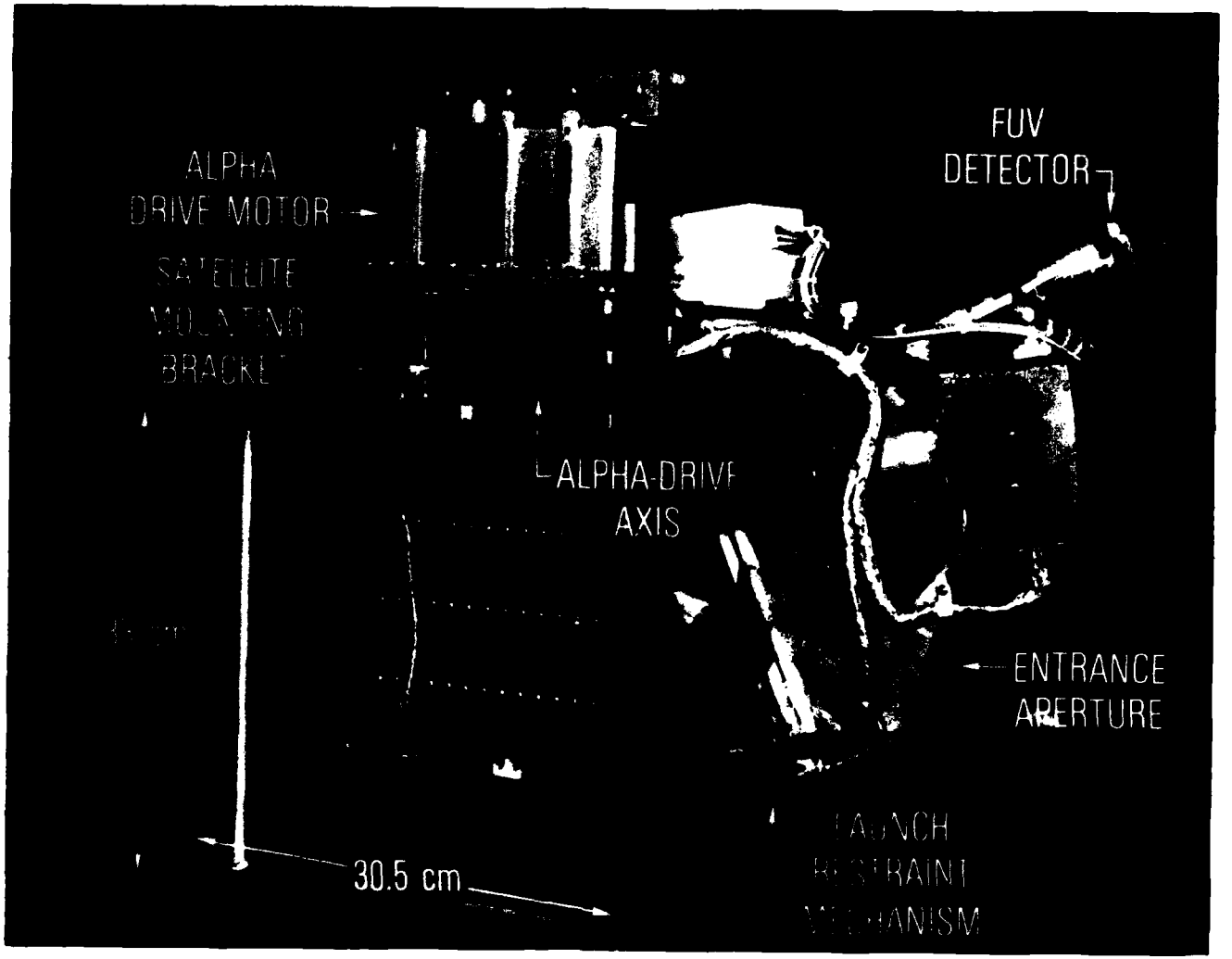

Fig. 3. Photograph of the SSD Instrument in a Laboratory Test Fixture

III. OPTICAL DESIGN

The major requirements on the optical design were: to measure weak atmospheric emission lines simultaneously in three ultraviolet wavelength bands; to achieve moderately high spectral resolution; to position the grating and the optical axis with mechanical systems capable of precise repeatability over an extended mission lifetime; to attain sufficient sensitivity with a narrow field of view and to attain these goals with a very severe weight limitation.

A Wadsworth concave grating spectrometer design was chosen to best satisfy these requirements. The single reflection design minimizes the severe EUV reflection losses. Collimation of the incident beam was provided by a mechanical collimator. By using the second and third diffraction orders for the EUV and FUV channels the system was made compact. This approach allowed effective use of the grating blaze to enhance the responsivity in all three wavelength bands.

Mechanical Collimator

A mechanical or modulation collimator of the McGrath (1968) type provides parallel light and defines the field of view of the instrument. It consists of an assembly of slotted grids, aligned and spaced in such a way that light can only traverse the assembly at small angles to the optical axis. As shown in Figure 4 the number of grids N and the spacing between them are chosen to block light incident to the optical axis at angles greater than the collimation angle θ, which is determined by the distance between the first and last grid (L) and by the width of the slots W. The parameters of the collimator are given in Table 1. The slots are interrupted by 3 bars which were required

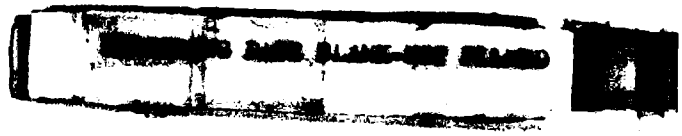

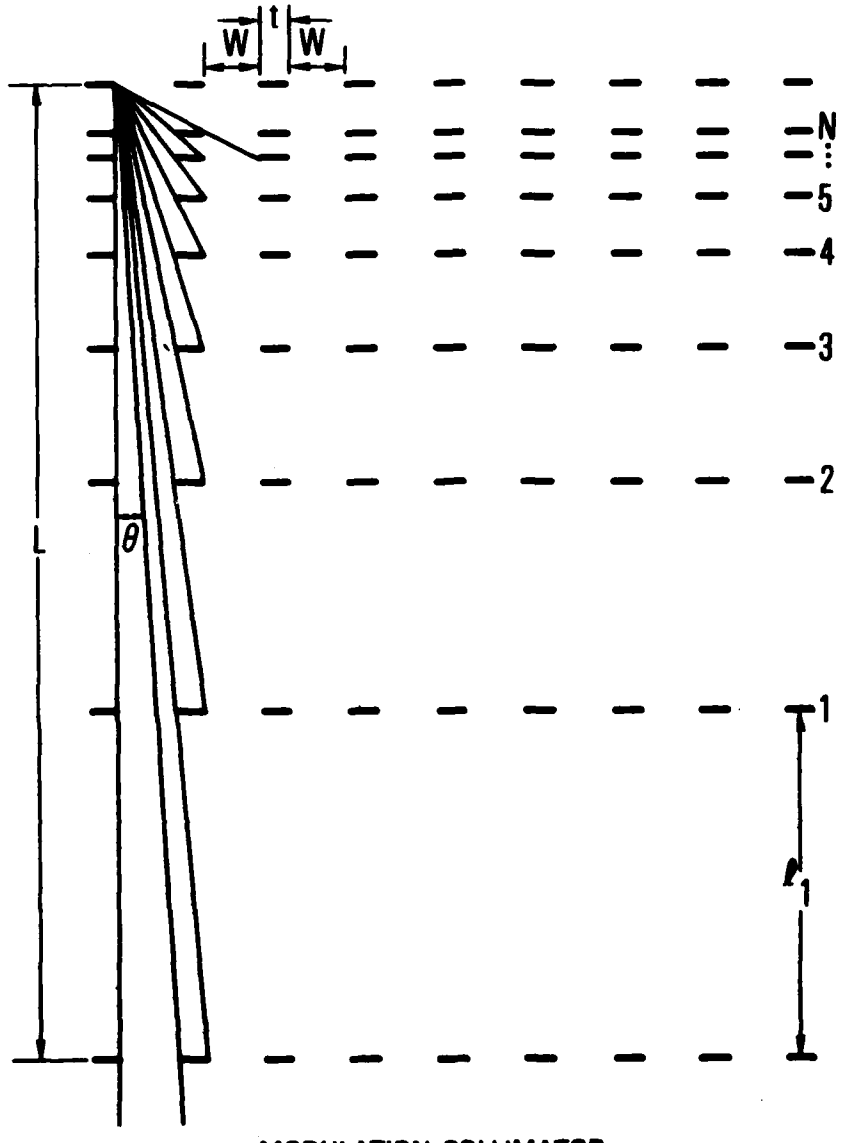

Fig. 4. Diagram of the Modulation Collimator. Two perpendicular collimators were used to define the SSD field of view. θ is the field of view defined by L/W where L is the collimator length and W the grid spacing.

Table 1. SSD Collimator Parameters

1.	Measured Field of View	0.14 x 3.75 degree FWHM (1.6×10^{-4} Ster.)
2.	Measured Aperture	14.8 cm^2
3.	Measured Transmission	27%
4.	Length	22.86 cm
5.	Number of Grids	13
6.	Number of Slots Per Grid	58
7.	Grid Thickness*	.005 cm
8.	Grid Material*	BeCu
9.	Grid Surface Treatment	Black Anodized

* 0.14° collimator

to strengthen the grids.

The 3° orthogonal field of view is provided by an additional collimator placed between grids 12 and 13. This collimator is made of 13 plates 5.398 cm long separated by spaces of 0.285 cm. The plates are black anodized aluminum 3.556 cm wide and 0.025 cm thick.

Grating

A tripartite concave grating (Hyperfine, Inc.) ruled at 1800 l/mm with a 498.1 mm radius is used with a platinum overcoat to maximize the response in the EUV; this, however, reduces the long wavelength efficiency. The ruled area is 54 x 54 mm and the grating is blazed at 300 nm in first order.

The grating is mounted to the grating drive mechanism by a three point kinematic system. The grating drive is mounted to precision mounting pads in the optics box using a three point kinematic mounting system. The incoming light is incident on the grating at 34° with the grating normal passing through the channel 1 (EUV) detector. The total grating rotation is ± 5°. A commandable heater is attached to the back of the grating to drive off condensation on the grating from outgassing of the SSD and the spacecraft during flight.

Slits

Three curved exit slits are mounted in a slit holder which in turn is mounted to a precision mounting pad in the optics box. There is a slit for each of the three orders so that emissions at 101.8 nm, 135.6 nm and 337.1 nm are observed at the same time for a fixed grating position. The EUV slit is placed on the grating normal to make use of the astigmatic and coma-free

features of the Wadsworth mounting. The slits are made from .0025 cm thick stainless steel etched from both sides.

Dichroic Mirror and Filter

A dichroic mirror (Infrared Industries, Mass.) having less than 5% reflectance for wavelengths less than 560 nm is used to direct the zero order beam to the NaD detector. An interference filter centered at 589.0 nm with a bandpass of 5.7 nm isolates the NaD emission lines.

Detectors

The set of photon counting detectors is described in Table 2.

Scattered Light and Light Leaks

Almost all of the surfaces and parts used in the optics box were treated with a black oxide coating or were painted black using 3M, Nextel Brand Velvet Coating, series 401-C10, which is a low outgassing, two part epoxy paint having a very low reflectance value from the EUV through the visible region of the spectrum. These materials were selected following an extensive study of UV reflection efficiencies of coatings suitable for spacecraft applications. The tests were performed by shining a monochromatic beam on the samples at an angle of incidence of 34°. The reflectance was measured from 23° to - 72° at four wavelengths and the peak value are listed in Table 3.

Light scattering was reduced with a light baffle between the grating cavity and the detector cavity which limited the fields of view of the detectors. The area between the light baffle and the slit mount was enclosed in an additional set of baffles to minimize scatter in this region and a baffle

Table 2. Detector Characteristics

Channel	Type	Window	Voltage	Gain	Manufacturer
1. EUV (85-120 nm) $\Delta\lambda$ = 0.4 nm	Channel Electron Multiplier (CEM)	Windowless	+3000 VDC, -50 VDC cone bias	9.5×10^7	Galileo Electro Optics Corp. Sturbridge, Mass.
2. UV (290-395 nm) $\Delta\lambda$ = 1.2 nm	541N-03-14-20000 (bi-alkali)	9741 glass	-2020 VDC	1.5×10^6	EMR Photoelectric Princeton, N. J.
3. NaD (589.0-589.6 nm)	510E-01-13-03900 (tri-alkali)	7056 glass	-1640 VDC	5.6×10^5	EMR
4. FUV (110-163 nm) $\Delta\lambda$ = 0.8 nm	542J-08-19-03900 (potassium bromide)	magnesium fluoride	-2210 VDC	1×10^6	EMR

Table 3. Results for EUV Low-Reflectance Surface Coatings

Item	Coating	Substrate Material	Reflectance % $\theta_i = 34°$; $-72° > \theta_R < 23°$ 91.3 nm	101.8 nm	135.6 nm	200.0 nm	Comments
1.	Martin Marietta Black Process	~10 Mil Al	0.02	0.02	0.025	0.035	
2.	Martin Marietta Black Process	~15 Mil Al	0.025	0.013	0.016	0.04	
3.	Martin Marietta Black Process	~ 5 Mil Al		0.27	0.47	0.55	Peak Near Normal
4.	3M 101-C10	Al	0.03	0.03	0.03		
5.	3M 101-C10	Al, Sand-blasted	0.07	0.34	0.23		Some Structure
6.	None	Al	1.78	1.90		16.74	Large Specular Peak
7.	None	Al, Sand-blasted	0.04	0.05	0.06	0.07	
8.	Chrome Black	Al, ?	0.032	0.02	0.024	0.037	Sample #8
9.	Chrome Black	Al, ?	0.015	0.075	0.017	0.031	Sample #11
10.	Chrome Black	Al, ?	0.028	0.034	0.033	0.052	Sample #12
11.	3M 401	Al	0.03	0.03	0.03	0.05	Lower Outgassing than C10 Series
12.	3M 401	Al, Sand-blasted	0.024	0.02	0.02	0.024	
13.	Black Anodized	Al	0.51	0.46	0.59	0.65	Specular Peak
14.	Black Anodized	Al, Sand-blasted	0.054	0.028	0.050	0.07	
15.	Chemglaze	Al, Sand-blasted	0.07	0.07	0.07	0.07	
16.	Chemglaze	Al	0.26	0.22			Peak Near ~ 66°
17.	Aquadag		0.18	0.12	0.13		Broad Peak Center ~ -20°
18.	Finch Cat-A-Lac Black	Al	0.21	0.18	0.18	0.20	Broad Specular Peak
19.	Finch Cat-A-Lac Black	Al, Sand-blasted	0.20	0.19	0.25	0.25	Broad Specular Peak

between the EUV detector and the FUV detector helped reduce scattered light in the detector cavity.

Access ports were sealed with gaskets of General Electric RTV 566. This is an opaque, low outgassing two-part silicone rubber compound.

IV. MECHANICAL DESIGN

Lambda Drive Assembly

The wavelength drive assembly consists of two DC brushless, space rated, Inland Motor Corporation torquers mounted on a common center of rotation with a tachometer and a custom-designed Inductosyn (Hartford, Conn.) position transducer. In the flight configuration the shaft is mounted on ball bearings; a lengthy effort to qualify a unit using Bendix flexures was not successful, due to size limitations.

The assembly is mounted in the optics box using a kinematic mount with the usual cone, ball, and groove three-point geometry. This allows alignment of the assembly relative to the other elements of the optical system.

The grating drive is caged for support during launch operations. The cage is released by the firing of redundant Holex cable cutters. Once the cables are cut, the caging pins are withdrawn by springs.

The major mechanical difficulties with this unit arise because it is an unbalanced assembly; the unbalance causes vibration stresses to appear as rotational torques. It would have been far better to accept the weight penalty and design for balanced rotational masses. However, the weight restriction imposed was a severe one and difficult choices were made to abide by it.

There is no momentum compensation on this axis since the inertia is small enough to fall below the limitation imposed by spacecraft requirements.

Alpha Drive Assembly

The alpha drive assembly rotates the entire optics box assembly in an earth limb scan. This is accomplished within a sealed unit by rotating a preloaded ball nut assembly to extend and retract a ball screw, thus rotating the optics box assembly via a crank mechanism.

The crank was designed as a discontinuous spring which limits vibrational loads by deflecting whenever the rotational torque exceeds a fixed threshold level. The servo action makes use of an Inland torque motor for a driver, an Inland tachometer for velocity feedback, and a linear potentiometer for position feedback. A small flywheel is coupled via step-up gearing to provide the required momentum compensation. Flexure supports were used to allow the small angular freedom needed in a mechanism of this type.

A shutter position is provided at the maximum rotation of the alpha drive. As the alpha box rotates into the shutter position, it pushes on an actuator arm which drives a shutter in front of the three exit slits and allows for a measurement of detector dark count levels.

Optics Box Assembly

The optics box assembly was one of the more difficult program developments. The minimum weight criteria led to the use of 1/32 in. sheet aluminum and a dip brazed construction.

The optics box alpha drive is caged during launch with a system of balls, ball socket joints, levers, a cable, and explosive cable cutters. It is necessary to custom fit the balls and sockets so that both balls exactly contact their respective sockets at the same alpha angle. This procedure insures that the loads induced by launch or vibration testing are carried by the two points of the restraint system equally.

V. ELECTRONIC DESIGN

A block diagram of the SSD logic system is shown in Figure 5. The instrument was interfaced with the spacecraft for command and power functions and with the prime payload instrument, the operational line scan system (OLS), for data exchange as shown in the interface drawing of Figure 6.

The Control System

The instrument receives instructions from both hard-wired circuits in the instrument and uplinked or stored commands from the spacecraft. As shown in Figure 5, binary commands are passed through a spacecraft/instrument buffer into the instrument command electronics which decodes the incoming binary stream into a 4-bit operating code word and a data word that specifies the particular instrument values such as the wavelength positions and alpha position to be used. The sequence controller acts as the main instrument controller providing sequencing and timing for the wavelength and alpha scanning mechanisms.

The integrated circuit (I.C.) memory contains a hard-wired code which takes effect on power-up of the instrument. This system is preempted by commands from the spacecraft.

The Alpha Scan System

The alpha drive circuit takes the form of a DC feedback position servo. The torque motor is driven by a DC amplifier which is in turn fed by signals from the error amplifiers and the rate feedback preamplifier and tachometer. Position information is fed into this circuit from the position potentiometer,

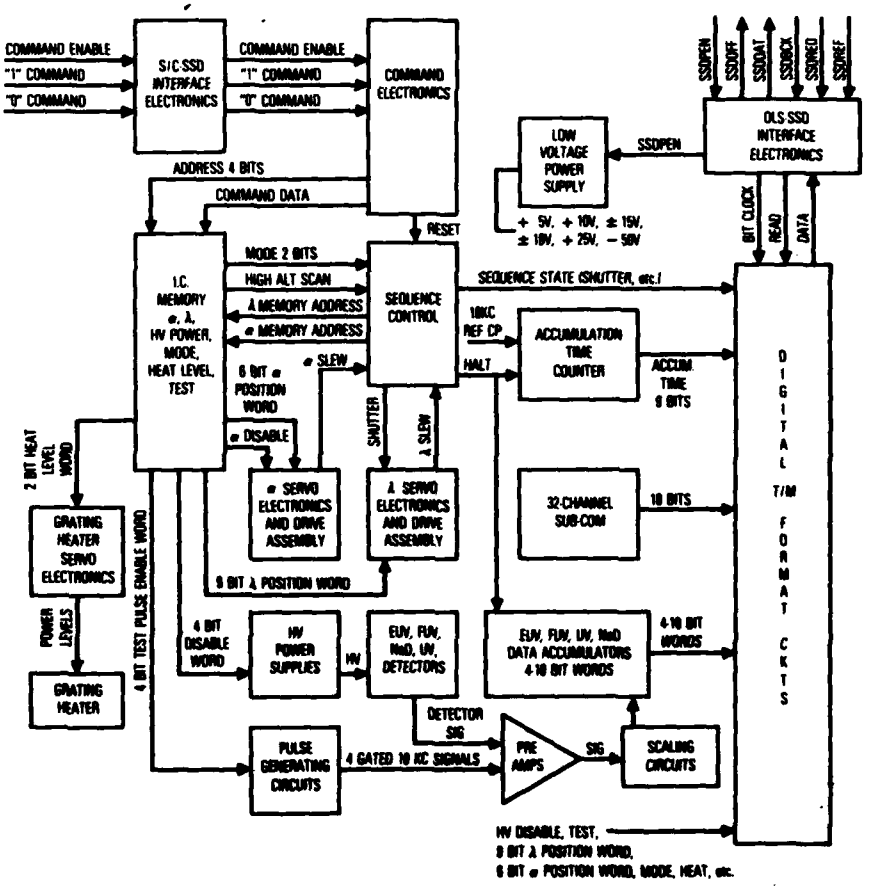

Fig. 5. Block Diagram of the SSD Logic Circuits

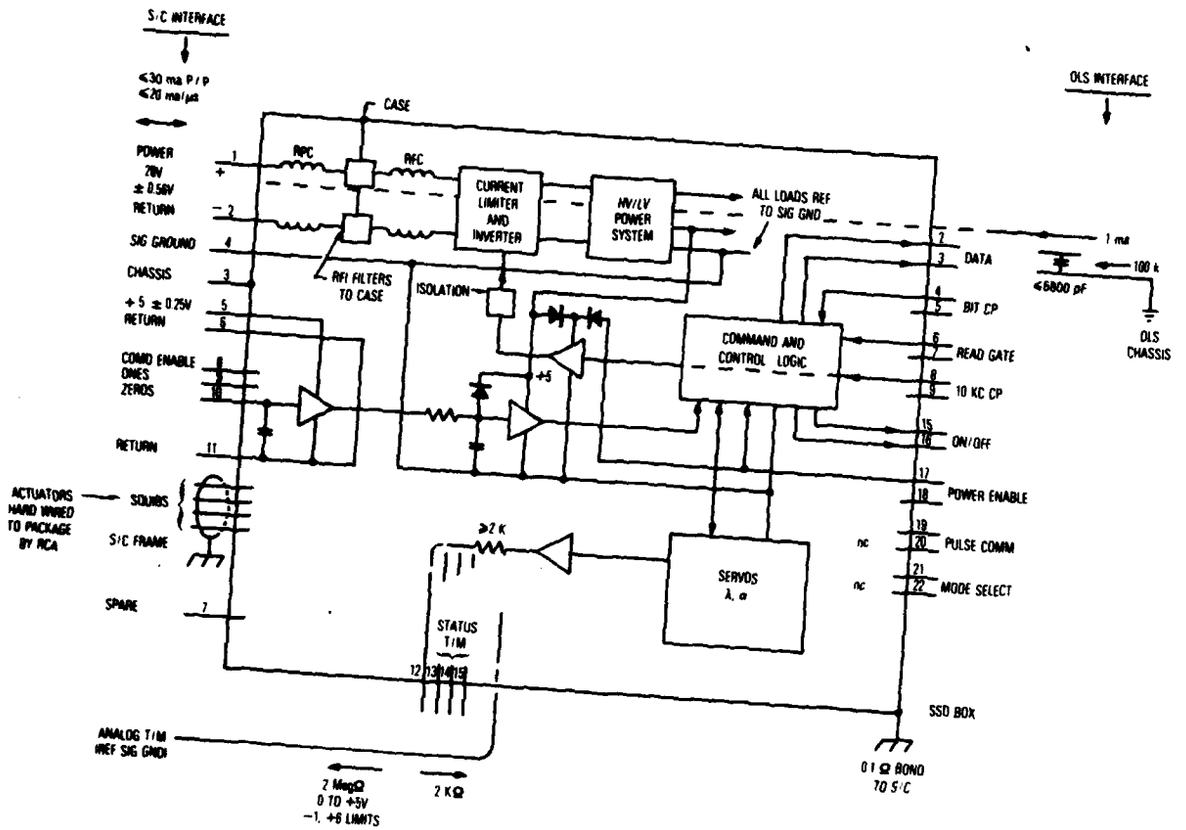

Fig. 6. Interface Diagram Showing the Spacecraft and OLS (Operational Line Scan System) Interface Connections to the SSD Instrument

which is a linear cermet-element potentiometer connected across the circuitry's 5 volt power bus. The stiffness and transient response of this position servo are sufficient to position the optics assembly to its final angle within about 50 milliseconds after a step of position change is introduced, if the change in position is less than about 5% of full scale. Larger steps demand a longer linear run in position before this settling phase occurs, with the result that the worst delay of a slew from one end to the other of the alpha scale is about 1 second. The power used to actuate this drive system is developed by the power supplies which deliver potentials of +18 and -18 volts at a power level of up to 18 watts. The current demand on this power bus is monitored by the telemetry system.

A monitor circuit used for determining the state of the error signals in the alpha loop is able to signal to the digital control system if the alpha axis is not within a satisfactory error angle of the command position. This signal takes the form of a logic level entitled "Alpha Slew". While this bit is true, the digital section is caused to register the interval as a counting loss interval so that detector data are not erroneously included for a time when the alpha axis is in motion. If the axis were to stick, this logic bit also supplies a warning of the condition, although in such a case a permanent data stoppage is not generated.

Lambda-Scan System

The angular position range of the grating motion is approximately 10° and is quantized into 512 steps by the command register. Thus, position angle is resolved to just over one arc minute (1.17 mins) of rotation. Knowledge of the angle to this resolution is developed by an angular sensor called an Inductosyn, which is essentially a rotary transformer, excited at 50 kHz by a

sinusoidal two-phase signal source. A combination of position and velocity signals is used to control the torque motor drive amplifier. Command signals for position angle are introduced from the digital reference source via a D to A converter. The stiffness and transient response of this servo are such as to position to any commanded angle within the 10 degree range within a settling time of approximately 25 milliseconds.

The power used to operate this lambda system is +15 and -15 volts at a power level of up to 15 watts. The current demand on this power bus is monitored by the telemetry system.

A monitor circuit used for determining the state of the error signal in the lambda loop is able to signal to the digital control system if the lambda axis is not within a satisfactory error angle of the command position. This signal takes the form of a logic level entitled "lambda slew" and serves the same function as "alpha slew".

The Power System

The power system consists of the following: four high-voltage supplies for the detectors, one supply which supplies ±15 volts for the low power analog systems and +25 volts to operate the high voltage supplies from a source at the correct ground reference, one +5 volt supply for a back-up clock, and two power sources for the alpha and lambda servos. The low voltage power supply contains a power monitor circuit so that the current demand on each of the four is measured and included in telemetry.

VI. MODES OF OPERATION

Operational control of the instrument is very flexible with both the alpha drive and the lambda drive having eight modes of operation which are selectable by ground command as listed in Table 4. Up to four alpha positions and four lambda positions may either be selected from values hard wired in the instrument or uplinked from the ground and stored in the instrument's memory.

The three principle operational modes are 0, 1 and 5. Mode 0 is the wavelength scan mode. The instrument views the limb at an angle specified by α_0 and the grating is stepped through each of its 512 positions providing a complete wavelength scan. At the end of the wavelength scan, a shutter-closed sequence is executed and the scan is repeated for α_1. The sequence is repeated until a mode change command is received.

Mode 1 executes a complete limb scan at each of four wavelength positions. The α position is stepped from a tangent height of ~ 80 km upward one α step at a time. At each α position, the λ drive positions the grating at the four λ positions. The scan requires 4 seconds per α position or approximately 160 seconds for the complete scan of 40 α positions.

Mode 5 allows observations at four α and four λ positions. The sequence requires only about 20 sec and therefore provides much better latitudinal resolution at the expense of altitude resolution. There is no shutter-closed sequence in this mode.

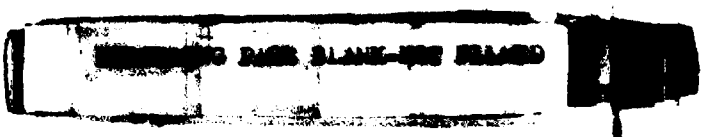

Table 4. D-Sensor Modes of Operation

Mode	Limb scan operation α_i refers to a stored α^i position	Grating scan operation. λ_i refers to a stored λ^i position	Variants
0	α_0, α_1, α_2, α_3	all 512 λ positions	
1	all α	λ_0, λ_1, λ_2, λ_3	high altitude disabled
2	all α	λ_0, λ_1	high altitude disabled
3	all α	λ_0	high altitude disabled
4	α_0	λ_3	
5	α_0, α_1, α_2, α_3	λ_0, λ_1, λ_2, λ_3	
6	α_0, α_1, α_2, α_3	λ_0, λ_1	
7	α_0, α_1, α_2, α_3	λ_0	

Note: Not all α_i and λ_i need be different.

VII. CALIBRATION

Various calibration techniques were utilized to determine the responsivity of the instrument across its wavelength range. In the vacuum ultraviolet, the calibration was carried out at the Laboratory for Atmospheric and Space Physics (LASP) at Boulder, CO, using a collimated ultraviolet beam from a monochromator. The beam intensity was monitored using a calibrated photomultiplier tube. The results are listed in Table 5 at wavelengths of principal interest.

The UV and NaD channels were calibrated using a tungsten iodide standard irradiance lamp (Optronics Model 200C, S/N-301) arranged to illuminate in turn a barium sulfate and magnesium oxide coated screen that filled the field of view of the instrument.

The responsivity of the EUV (channel 1) was determined by measuring separately the grating efficiency, the transmission of the collimator, the quantum efficiency of the channel 1 detector, the instrument aperture, and field of view.

Grating Efficiency

The grating efficiency is the product of the grating reflectivity and the efficiency of the blaze, i.e.,

$$\eta = R(\lambda) * \epsilon(\theta),$$

where the reflectivity (R) is assumed to be only a function of the wavelength (permissible for the small angles of incidence in the SSD spectrometer) and

Table 5. D-Sensor Responsivity at Selected Wavelengths

Channel	Wavelength (nm)	Responsivity (cts/sec R)
2	337.1	4.0×10^{-1}
3	589.0	4.8×10^{-2}
4	135.6	8.4×10^{-2}
4	130.4	1.5×10^{-1}
4	132.5	1.3×10^{-1}
4	121.6	1.3×10^{-1}

the blaze efficiency ε is assumed to be dependent only on the diffraction angle.

The grating efficiency was measured using light in the 80 nm to 120 nm region. The reflectivity of the grating was determined by summing the light diffracted in all orders from n = -3 to +4. In this wavelength range the reflectance was 17 ± 1%, consistent with the normal incidence values given in Samson (1967) for platinum. The resultant blaze efficiency curve is plotted in Figure 7 as a function of the first order wavelength.

The polarization properties of the grating were measured in the near ultraviolet using a linear polarizing filter and a quartz-iodide lamp. The lamp polarization was less than 1%. From minimum to maximum grating angle the polarization varied from 40% to 60% which gives a sensitivity of the instrument 2 to 4 times greater to light with parallel polarization.

Detector Quantum Efficiency

The quantum efficiency of the flight photomultipliers is shown in Figure 8. The photomultiplier values were supplied by the manufacturer (EMR). The quantum efficiency of the channeltron used for the EUV detector was calibrated with monochromatic light against a windowless National Bureau of Standards photodiode having an Al_2O_3 photocathode.

α-Scan

The repeatability of the α-scan drive was measured several times during the evaluation and testing phase of the instrument development. The drive mechanism was shown to position the instrument to a precision of ± 1 minute of arc. Table 6 lists the α-step number and the corresponding depression angle of the line of sight.

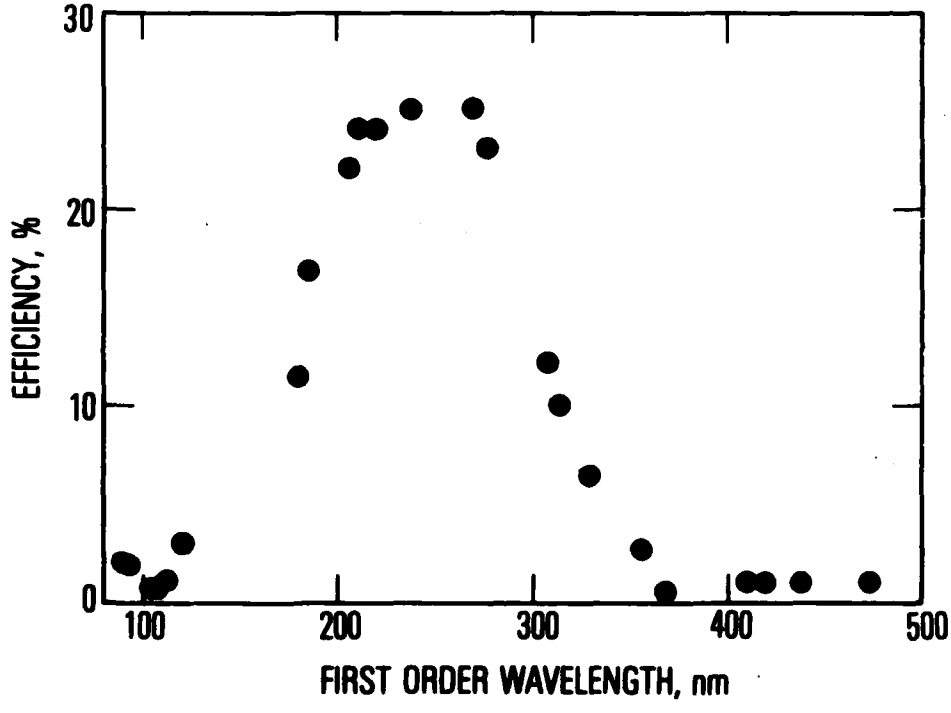

Fig. 7. Measured Blaze Efficiency of the SSD Flight Grating #233-4-2 Expressed as a Function of First-Order Wavelength. Grating overcoat was platinum.

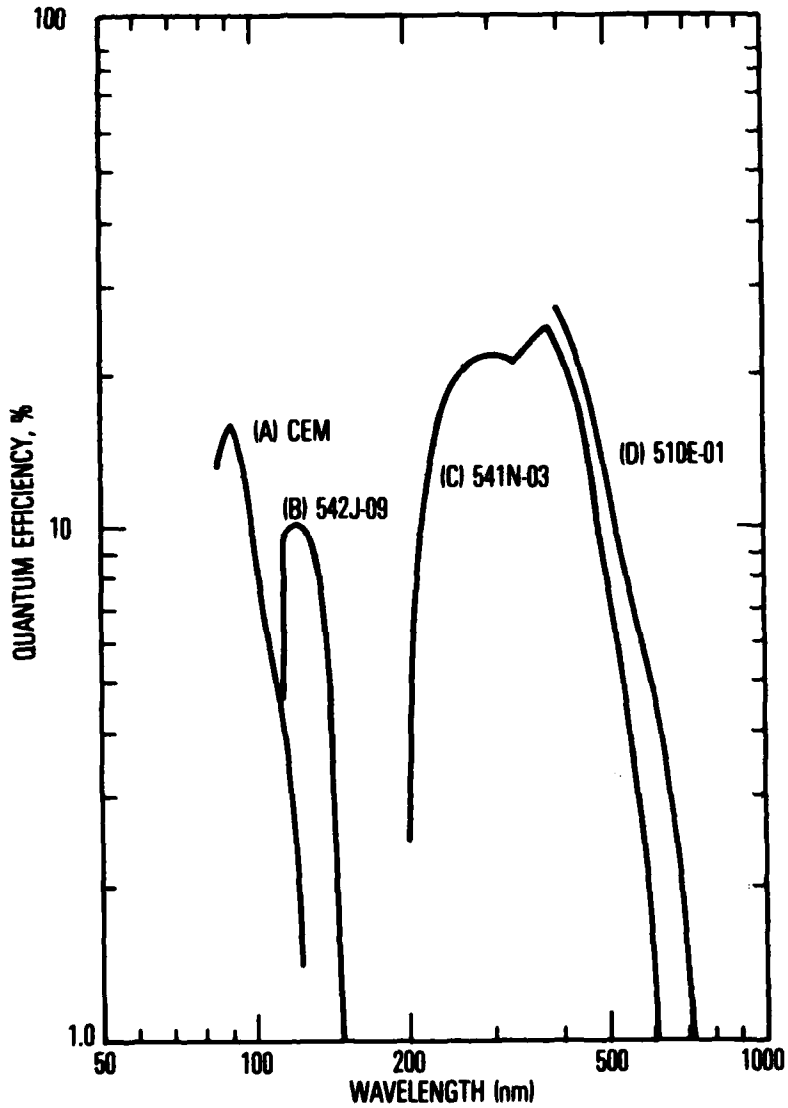

Fig. 8. Quantum Efficiencies for the Four Detector Channels. The channeltron values were measured in our laboratory. PMT values were supplied by the manufacturer (EMR, Princeton, NJ).

Table 6. α-Scan Depression Angles in Degrees

Step #	α	Step #	α	Step #	α	Step #	α
0	26.54°	11	25.09°	22	23.66°	39	21.26°
1	26.46	12	24.97	23	23.48	43	20.73
2	26.33	13	24.86	24	23.34	47	20.27
3	26.20	14	24.72	25	23.22	51	19.72
4	26.06	15	24.58	26	23.08	55	19.27
5	25.92	16	24.47	27	22.95	59	18.72
6	25.78	17	24.32	28	22.83	63	18.16
7	25.64	18	24.17	29	22.72		
8	25.51	19	24.05	30	22.54		
9	25.36	20	23.89	31	22.40		
10	25.22	21	23.78	35	21.84		

λ-Scan

The wavelength scanning mechanism was also verified from time to time prior to launch and the alignment was verified on-orbit through observation of the strong airglow lines in the far-ultraviolet. The shift in position amounted to about one wavelength step. No shifts have occurred in the wavelength drive since the instrument was first turned on. Spectral line widths in flight were identical to pre-flight calibrations.

VIII. FLIGHT DATA

The initial on-orbit operations were intended to check each of the operating modes. The mode 0 wavelength scan requires 8.5 min to complete, so it is not practical to operate in a wavelength scanning mode for spatial studies of the atmospheric emissions. It was used to verify wavelength calibration and stability so that in normal operations the instrument could be set on particular wavelengths of interest and scanned in altitude.

An example of mode 0 wavelength scan data is shown in Figure 9 for the FUV channel. The principal emission lines NI(120.0 nm), H Lyα (121.6 nm), OI(130.4 nm), OI(135.6 nm), and N_2 LBH bands are clearly evident in a single λ-scan viewing a tangent height of 210 km in the sunlit atmosphere. Both the grating efficiency and the detector quantum efficiency contribute to the rapid loss of responsivity at the longer wavelengths.

Figure 10 is a composite of ten wavelength scans obtained with the EUV detector. The wavelength scale is for the 3rd order; however, features are evident from the second through the sixth order. The spectrum does not have the appearance of the normal first order spectra such as published by Christensen (1976), or Gentieu et al. (1979), due to the overlapping orders and the viewing geometry.

The best mode of operation for atmospheric density determination is mode 1, where the instrument scans the complete altitude range at four wavelengths. In Figure 11 are shown the results of a mode 1 scan with the FUV channel set to observe OI(130.4 nm), OI(135.6 nm) and LBH(4,0). The fourth wavelength was a background channel near 134.0 nm. The altitude profiles in the three emissions are plotted in terms of signal count rate versus the

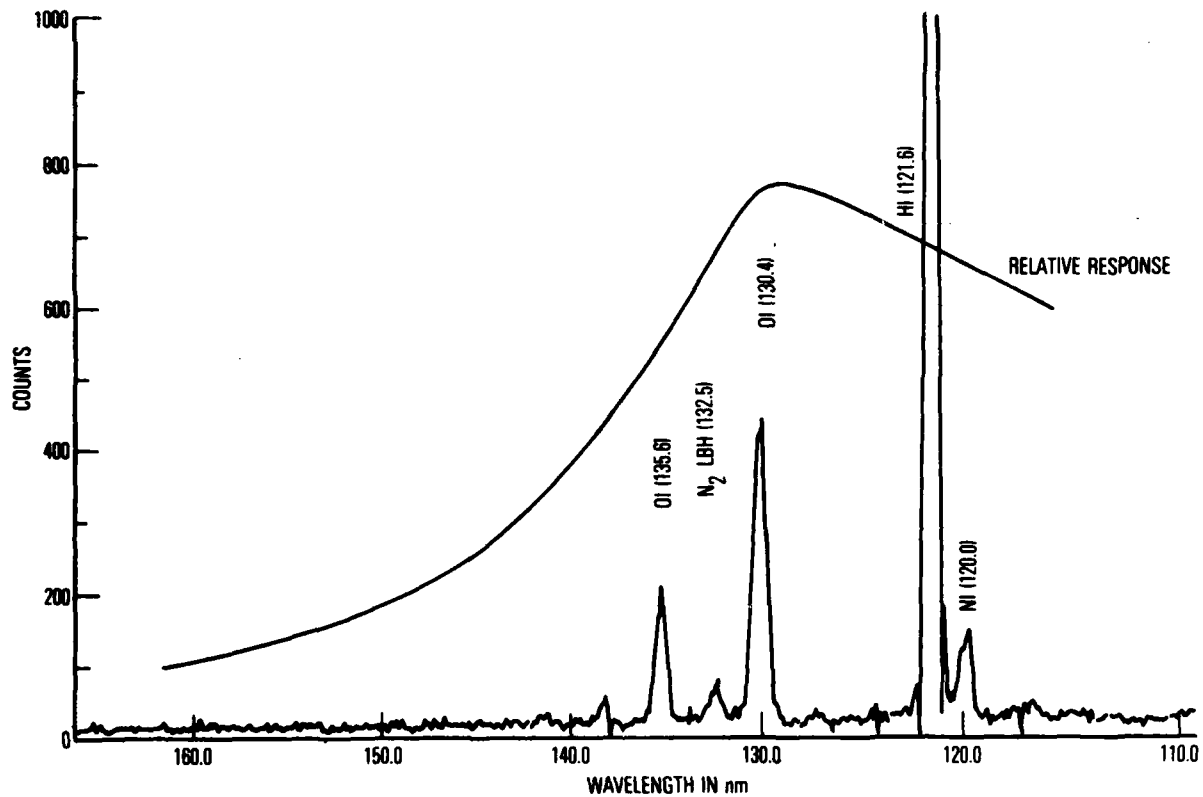

Fig. 9. Single Wavelength Scan of the Far Ultraviolet Dayglow (110-160 nm) for a Tangent Height of 210 km Obtained on Day 169 (18 June 1979). Satellite latitude 70-81° N, longitude 134-232° E, Rev. #163, UT 2.5 h.

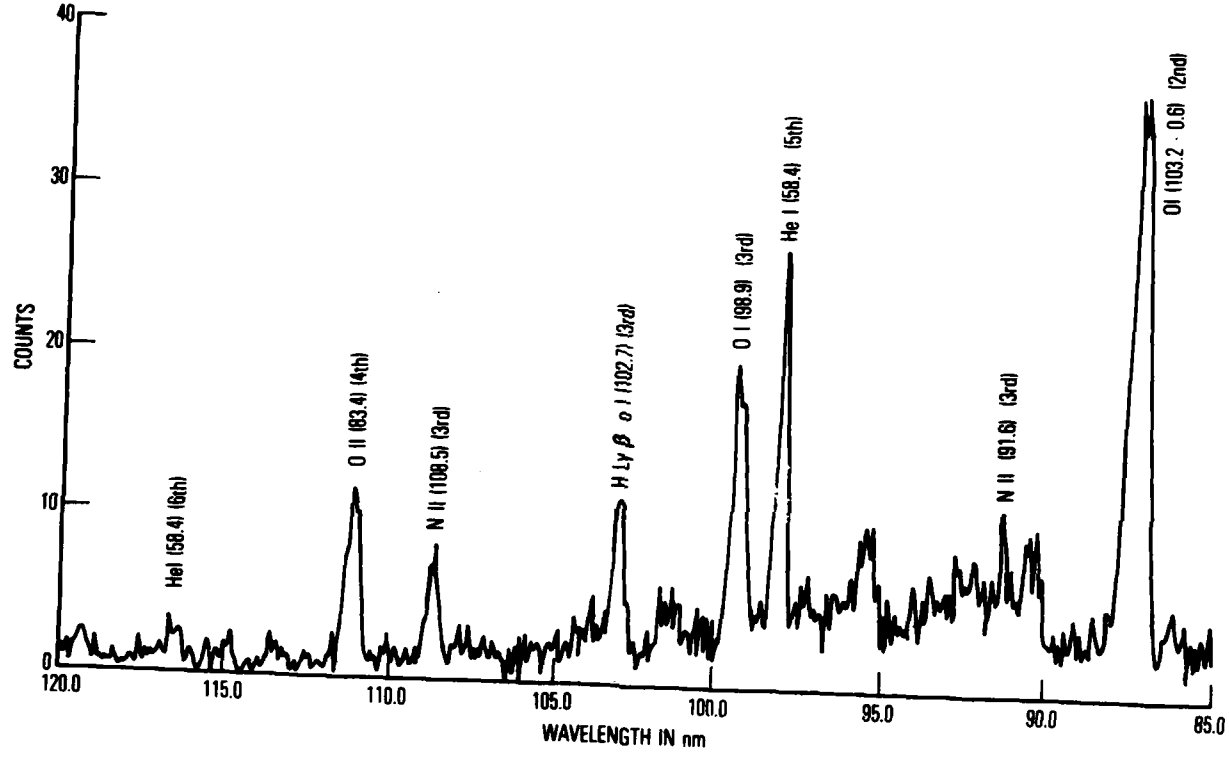

Fig. 10. An EUV Composite Spectrum of the Dayglow Obtained by Summing Spectra from Several Target Altitude and Satellite Locations. The wavelength scale is for third-order diffraction. Some higher-order features are identified.

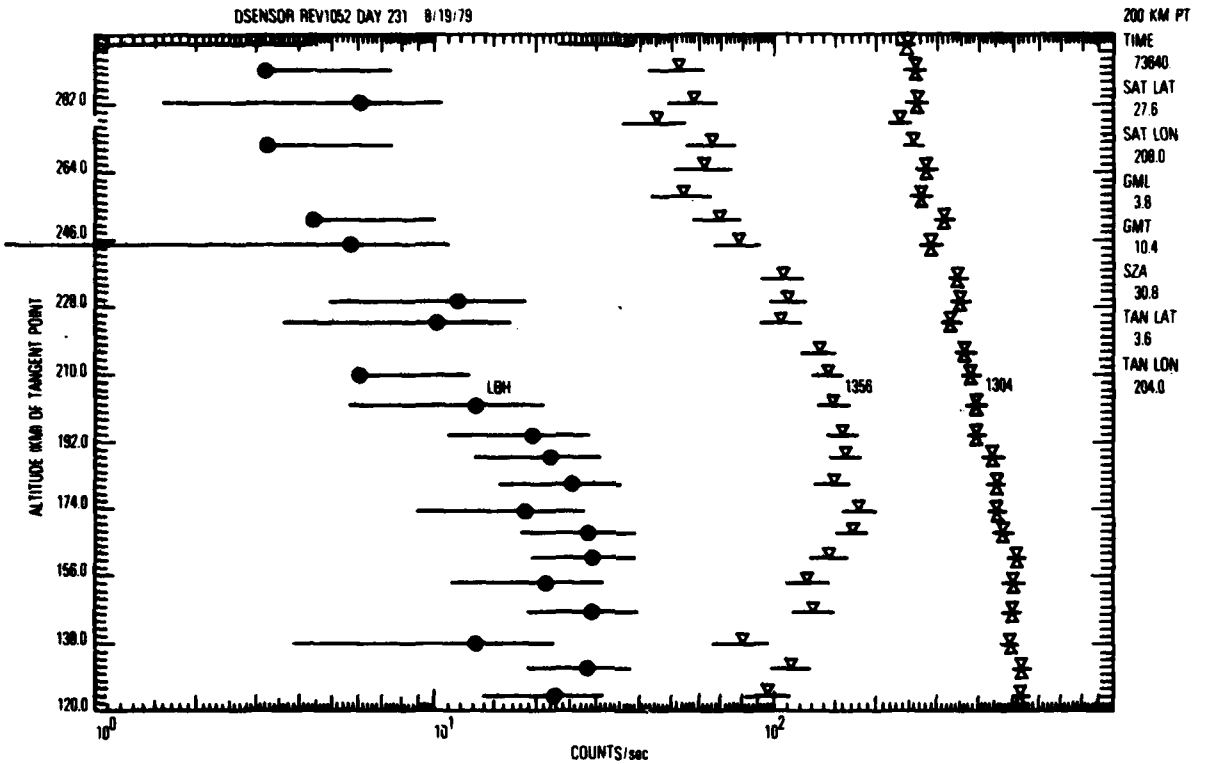

Fig. 11. Single α-Scan Mode 1 Data for the Atomic Oxygen Emissions OI(130.4 nm) and OI(135.6 nm) and the Molecular Nitrogen LBH(0,4) Emission at 132.5 nm. Count rates are plotted versus the altitude of the tangent point. Uncertainties due to counting statistics are shown with horizontal bars except when the end points are negative. The legend lists the time of the observation nearest the 200-km tangent height in seconds UT, the satellite latitude and longitude, the geomagnetic latitude and time of the tangent point, the solar zenith angle and geographic latitude and longitude of the tangent point.

tangent point altitude over the range of 120 to 300 km. The standard deviations for each observation point are indicated except when the end points are negative, as is the case for some of the LBH values (introduced by background subtraction).

The contrast in the profiles of the atomic oxygen emissions is rooted in radiative transport effects. The vertical optical depth for the OI(130.4 nm) emission is 10^3 to 10^4 at these altitudes, giving rise to a very slowly varying limb intensity. The LBH emission is optically thin and falls off much faster at high altitude following the smaller N_2 scale height.

Nightside observations of mesospheric sodium emission are shown in Figure 12 for two scans of the layer at northern low latitude. The emission from the NaD doublet is seen to peak in the 75-80 km range, but other data suggest a latitudinal dependence of both the peak intensity and altitude of the peak associated with variations in the mesospheric ozone and atomic sodium distributions.

Figure 13 illustrates data obtained crossing the southern polar region for the most common operating mode of the instrument (Mode 5). In this mode, four selected wavelength positions are measured at four selected viewing angles. In Figure 13, the α positions 2, 6, 16, 59 refer to nominal tangent heights of 95, 125, 210 and 485 km, respectively. The time in seconds (UT), the latitude and longitude, and the solar zenith angle of each sub-satellite point are listed. The instrument views a tangent point approximately 26° ahead of the satellite. The Lyα(121.6 nm) data (13a) show emission insensitive to α, consistent with the large hydrogen scale height and multiple scattering. Aurora is clearly evident near 56758 sec. both in Lyα and in OI(130.4 nm) shown in Figure 13b. The differences between the signals, such

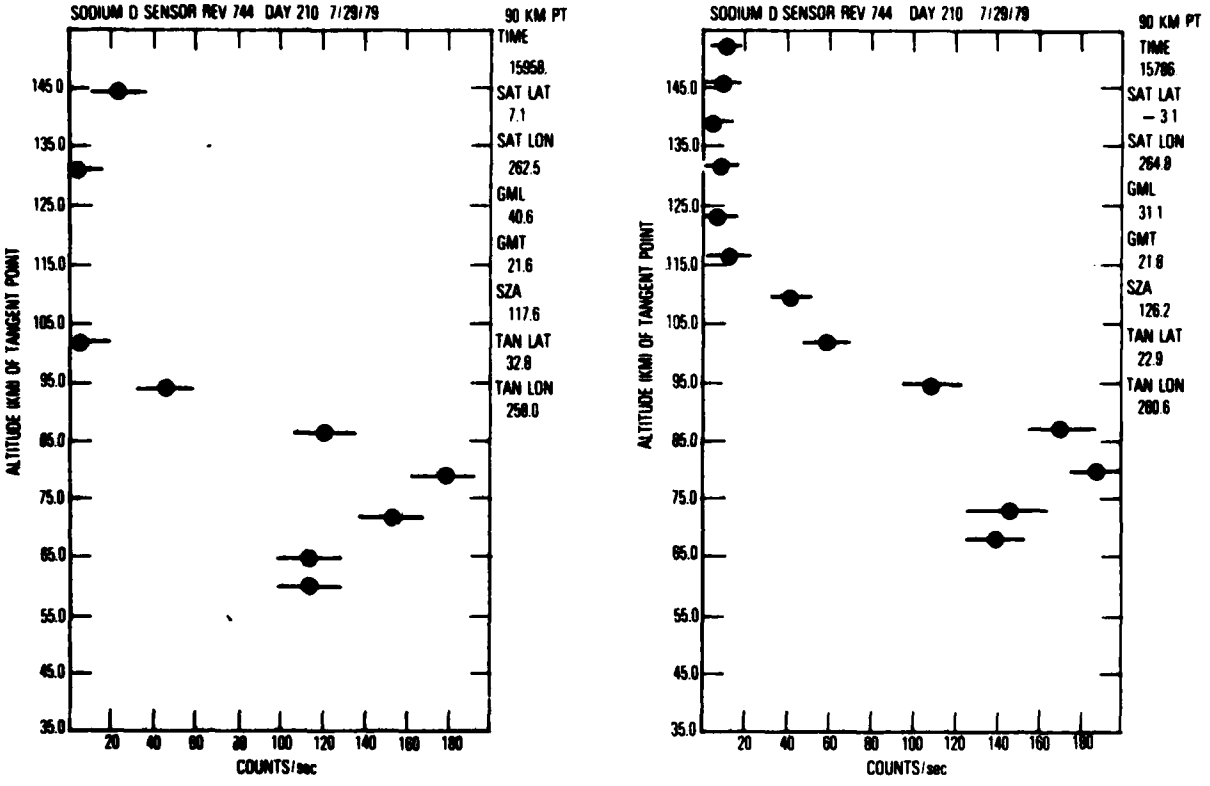

Fig. 12. Single α-Scan Data for Atomic Sodium (NaD) Doublet Emissions. Count rates are shown versus the altitude of the tangent point. The legend gives values at the 90-km tangent altitude with the same format as Figure 11.

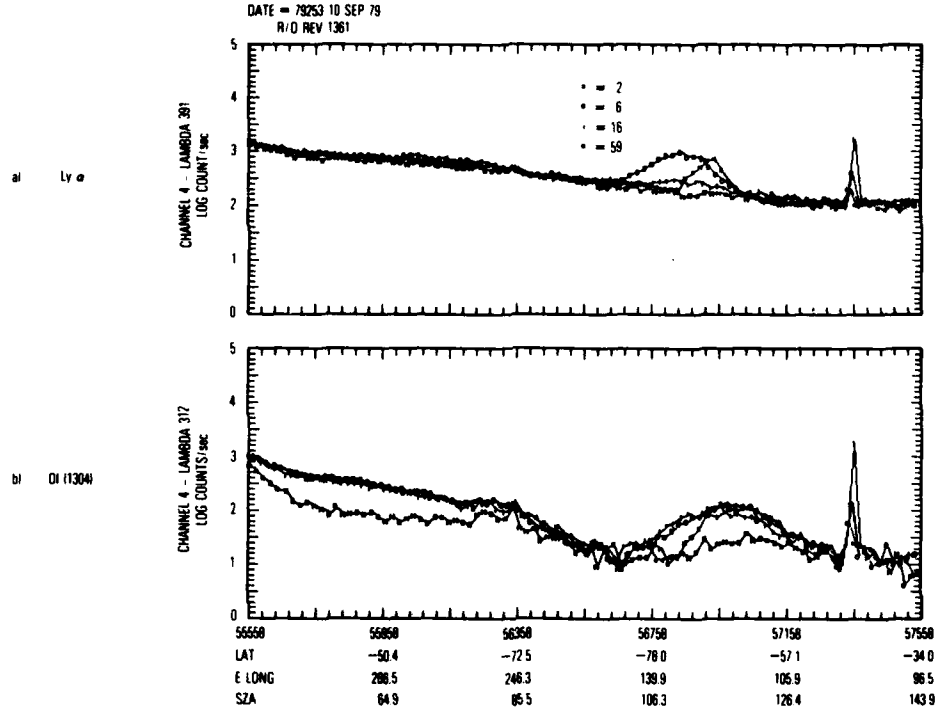

Fig. 13. Raw Count Rate Data from Day 253 (10 September 1979) with SSD Instrument in Mode 5, i.e., 4 Wavelength Positions at 4 Alpha Positions. Universal time in seconds, latitude and longitude in geodetic coordinates, and the solar zenith angle of the subsatellite point are given below each figure. Alpha step numbers correspond to nominal tangent heights of 95, 125, 210 and 485 km.

a) H Ly α (121.6 nm) intensity showing a southern auroral enhancement.

b) OI(130.4 nm) intensity showing passage across the terminator with an auroral enhancement displaced in latitude. The spike at 57358 s is due to direct sunlight on the entrance collimator.

as apparent width and intensity of the auroral enhancement, are dependent on the geographical extent, altitude and brightness of the localized emission region.

IX. CONCLUSIONS

The development of the SSD instrument has involved several significant challenges, mainly in the mechanical design area. The requirements for mechanical rigidity with repeatable control of the wavelength and altitude scan mechanisms in a system that would pass environmental shake tests were difficult to achieve under the severe weight restriction imposed by spacecraft considerations. As a result some on-orbit problems occurred that were due to our having compromised too much in some subsystems. However, the great flexibility of the instrument in the selection of modes, wavelengths, scanning angles, etc. has allowed us to obtain data of good quality so as to address some interesting basic research questions and problems associated with remote sensing of density.

References

Anderson, D. E., P. D. Feldman, E. P. Gentieu and R. R. Meier, "The UV Dayglow 3, OI Emissions at 989, 1027, 1152, 1304 and 1356 Å, " Geophys. Res. Lett. 7, 1057-1060, 1980.

Carruthers, G. R. and T. Page, "Apollo 16 Far-Ultraviolet Camera/ Spectrograph: Earth Observations," Science 177, 788-791, 1972.

Christensen, A. B., "A Rocket Measurement of the Extreme Ultraviolet Dayglow," Geophys. Res. Lett., 3, 221-224, 1976.

Doering, J. P., G. Fastie and P. D. Feldman, "Photoelectron Excitation of N_2 in the Day Airglow," J. Geophys. Res. 75, 4787-4801, 1970.

Gentieu, E. P., P. D. Feldman and R. R. Meier, "Spectroscopy of the Extreme Ultraviolet Dayglow at 6.5 Å Resolution: Atomic and Ionic Emissions Between 530 and 1240 Å," Geophys. Res. Lett., 6, 325-328, 1979.

Holland, R. F., "Excitation of Nitrogen by Electrons: The Lyman-Birge-Hopfield System of N_2^*," Jour. Chem. Phys. 51, 3940-3950, 1969.

McGrath, J. F., Jr., "New Technique for the Design of an Extreme Ultraviolet Collimator," Rev. Sci. Instr. 39, 1036, 1968.

Prag, A. B., private communication.

Samson, J. A. R., "Techniques of Vacuum Ultraviolet Spectroscopy," John Wiley & Sons, Inc., New York, 1967.

Zipf, E. C. and R. W. McLaughlin, "On the Dissociation of Nitrogen by Electron Impact and by EUV Photo-Absorption," Planet. Space Sci., 26, 449-462, 1978.

LABORATORY OPERATIONS

The Laboratory Operations of The Aerospace Corporation is conducting experimental and theoretical investigations necessary for the evaluation and application of scientific advances to new military space systems. Versatility and flexibility have been developed to a high degree by the laboratory personnel in dealing with the many problems encountered in the nation's rapidly developing space systems. Expertise in the latest scientific developments is vital to the accomplishment of tasks related to these problems. The laboratories that contribute to this research are:

Aerophysics Laboratory: Launch vehicle and reentry aerodynamics and heat transfer, propulsion chemistry and fluid mechanics, structural mechanics, flight dynamics; high-temperature thermomechanics, gas kinetics and radiation; research in environmental chemistry and contamination; cw and pulsed chemical laser development including chemical kinetics, spectroscopy, optical resonators and beam pointing, atmospheric propagation, laser effects and countermeasures.

Chemistry and Physics Laboratory: Atmospheric chemical reactions, atmospheric optics, light scattering, state-specific chemical reactions and radiation transport in rocket plumes, applied laser spectroscopy, laser chemistry, battery electrochemistry, space vacuum and radiation effects on materials, lubrication and surface phenomena, thermionic emission, photosensitive materials and detectors, atomic frequency standards, and bioenvironmental research and monitoring.

Electronics Research Laboratory: Microelectronics, GaAs low-noise and power devices, semiconductor lasers, electromagnetic and optical propagation phenomena, quantum electronics, laser communications, lidar, and electro-optics; communication sciences, applied electronics, semiconductor crystal and device physics, radiometric imaging; millimeter-wave and microwave technology.

Information Sciences Research Office: Program verification, program translation, performance-sensitive system design, distributed architectures for spaceborne computers, fault-tolerant computer systems, artificial intelligence, and microelectronics applications.

Materials Sciences Laboratory: Development of new materials: metal matrix composites, polymers, and new forms of carbon; component failure analysis and reliability; fracture mechanics and stress corrosion; evaluation of materials in space environment; materials performance in space transportation systems; analysis of systems vulnerability and survivability in enemy-induced environments.

Space Sciences Laboratory: Atmospheric and ionospheric physics, radiation from the atmosphere, density and composition of the upper atmosphere, aurorae and airglow; magnetospheric physics, cosmic rays, generation and propagation of plasma waves in the magnetosphere; solar physics, infrared astronomy; the effects of nuclear explosions, magnetic storms, and solar activity on the earth's atmosphere, ionosphere, and magnetosphere; the effects of optical, electromagnetic, and particulate radiations in space on space systems.

• • •

ATE
LME